Aldose Reductase as a Target for Drug Design: Molecular Modeling Calculations on the Binding of Acyclic Sugar Substrates to the Enzyme†

Hans L. De Winter and Mark von Itzstein*

Department of Medicinal Chemistry, Victorian College of Pharmacy, Monash University, 381 Royal Parade, Parkville 3052, Victoria, Australia

Received December 20, 1994; Revised Manuscript Received April 10, 1995®

ABSTRACT: In an attempt to obtain a picture of the binding conformation of aldehyde substrates to human aldose reductase (hAR), modeling calculations have been performed on the binding of three substrates, D-xylose, L-xylose, and D-lyxose, to wild-type human aldose reductase and two of its site-directed mutants. It was found that the average geometry of D-xylose in the active site of wild-type aldose reductase is characterized by strong hydrogen bonds involving the reactive carbonyl oxygen of the substrate and both Tyr48 and His110. The calculations also suggest the importance of Trp111 in the binding of 2′-hydroxyl-containing aldehyde substrates. A good correlation between calculated interaction enthalpies and experimental $\log(K_m)$ or $\log(k_{cat}/K_m)$ values was obtained when His110 was modeled with its Nε2 atom protonated and Nδ1 unprotonated. No correlation was found for the other two configurations of His110. On the basis of comparisons of the calculated substrate binding conformations for the three possible His110 configurations, and on the correlations between measured $\log(K_m)$ or $\log(k_{cat}/K_m)$ and calculated parameters, it is proposed that His110 is neutral and protonated at Nε2 when an aldehyde substrate is bound to the hAR/NADPH complex. A chain of three hydrogen-bonded water molecules has been identified in all available crystal structures and is located in an enzyme channel which links the Nδ1 atom of His110 to the solvent-accessible surface of the enzyme. A possible role of this channel in the mechanism of catalysis of aldose reductase is suggested.

Human aldose reductase (hAR),[1] an NADPH-dependent enzyme, catalyzes the reversible reduction of a wide variety of carbonyl-containing compounds to their respective alcohol counterparts (Flynn & Green, 1993; Wermuth et al., 1982). Human aldose reductase consists of a single polypeptide chain of 315 residues with a molecular mass of 35.8 kDa (Wilson et al., 1992), and its crystal structure was first solved by Wilson et al. (1992) and characterized in more detail by Harrison et al. (1994), who also solved the Y48H mutant structure (Bohren et al., 1994).

The active site pocket of hAR, 12 Å deep and approximately 10 × 10 Å square, is lined by seven aromatic and four other nonpolar residues and is therefore very hydrophobic. The only polar residues within the pocket are Cys298, Tyr48, and His110. The nicotinamide ring of the NADPH cofactor forms the base of the pocket, and the hydroxyl group of Tyr48 and the imidazole ring of His110 are positioned above it (Figure 1).

The catalytic mechanism of hAR appears to be relatively simple, involving the protonation of the substrate by an acid−base catalyst and a stereospecific transfer of the 4-*pro-R* hydrogen, presumably in the form of a hydride ion, from the C4 of the nicotinamide ring to the *re* face of the carbonyl carbon of the substrate. A similar stereochemistry for hydride transfer of the 4-*pro-R* hydrogen to the *re* face of the substrate carbonyl is observed in the closely related enzyme aldehyde reductase (Flynn et al., 1975). An important step in the mechanism is the transfer of a proton from a proton donor group in the enzyme's active site to the carbonyl oxygen of the substrate. Cys298, Tyr48, and His110 could all act as the proton donor; however, because Cys298 is not conserved in the aldo−keto superfamily, its role as a putative proton donor group in hAR is considered to be less likely (Bohren et al., 1989). Thus, only His110 and Tyr48 are presumed to be reasonable candidates.

Although a physiological role for this enzyme has not yet been established, inhibitors of hAR appear to be effective in the treatment of diabetic neuropathy (Masson & Boulton, 1990). However, many of these inhibitors present serious side effects (Kador, 1988), and these problems have fueled the search for less toxic and more specific hAR inhibitors. Our recent interest in hAR as a target for drug design has prompted us to study the enzyme at the atomic level. A detailed knowledge of the preferred binding conformations of hAR substrates is useful for the design of transition-state analogues and other potential inhibitors. Unfortunately, the direct observation of the binding conformation of substrates in the active site pocket of hAR has not yet been possible, presumably because of the difficulties in either crystallizing a suitable hAR/substrate complex or soaking substrate into crystals. In addition, knowledge of the tautomeric configuration of His110 in the active site of hAR is also crucial in the rational design of inhibitors because, depending on this residue's tautomeric configuration, it can be either a hydrogen bond donor or an acceptor. Unfortunately, the weak electron density around hydrogen atoms makes it impossible to locate, by X-ray diffraction, the position of hydrogen atoms in proteins. Thus, any experimental information concerning the protonation state of His110 in hAR is not available.

† This work was supported by a D. Collen Research Foundation (Leuven, Belgium) fellowship for H.L.D.W.

* To whom correspondence should be addressed.

® Abstract published in *Advance ACS Abstracts,* June 1, 1995.

[1] Abbreviations: hAR, human aldose reductase; NADPH/$NADP^+$, nicotinamide adenine dinucleotide phosphate, reduced and oxidized forms, respectively; K_m, Michaelis−Menten constant; k_{cat}, catalytic constant; MD, molecular dynamics; MM, molecular mechanics; ALR1, aldehyde reductase.

0006-2960/95/0434-8299$09.00/0

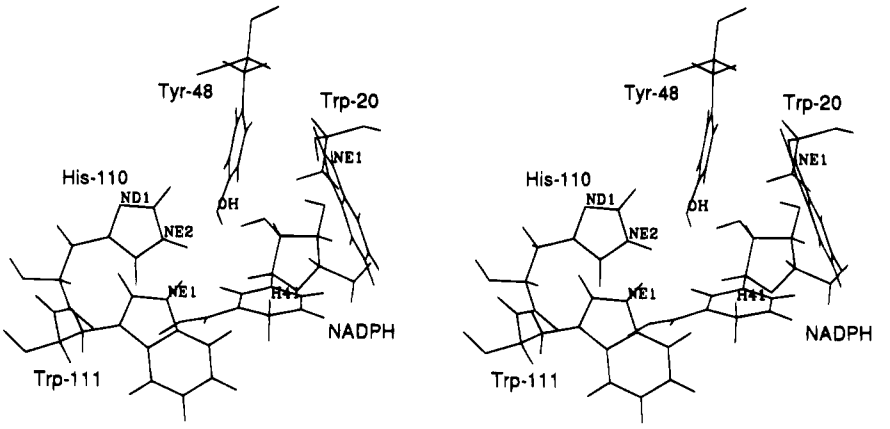

FIGURE 1: Stereo plot of the active site of hAR. The positions of the two likely proton donor candidates, His110 and Tyr48, relative to the cofactor's nicotinamide ring which forms the base of the active site are shown. His110 is shown with its Nε2 atom protonated and with Nδ1 unprotonated. The other tautomeric form, with only Nδ1 protonated, or the configuration with both nitrogens protonated, is not shown. Residues Trp20 and Trp111, two of the hydrophobic residues lining the active site pocket, are also displayed. The 4-*pro-R* hydrogen of NADPH (labeled as H41), which is positioned above the nicotinamide ring plane in this view, is transferred to the substrate's carbonyl carbon during the forward reaction catalyzed by hAR (reduction of carbonyl compounds).

On occasion, the likely tautomeric state of histidine residues can be deduced by inspection of the molecular environment of these residues in protein crystal structures. A good example is found in the crystal structure of the triosephosphate isomerase/phosphoglycolohydroxamate complex (Davenport et al., 1991), in which the main-chain amide of Glu97 donates a hydrogen bond to the Nδ1 of the active site His95. Therefore, this particular histidine residue must be neutral in the structure with the Nε2 atom protonated (Davenport et al., 1991). Unfortunately, in aldose reductase, such a deduction of the tautomeric state of His110 from pure steric and geometrical considerations of its molecular environment is not obvious because both nitrogen atoms of His110 are hydrogen bonded to water molecules. The Nε2 nitrogen of His110 is exposed to solvent in the active site, while the Nδ1 atom is hydrogen bonded to a chain of three water molecules which links the Nδ1 atom of His110 to the solvent-accessible surface of the enzyme.

This channel of three water molecules, present in all four crystal structures of hAR (Wilson et al., 1992; Harrison et al., 1994), starts at Nδ1 of His110 and slightly curves around the backbone of Lys77 and Leu78 to emerge at a surface dimple near His46, Tyr82, Lys94, and Asp98. A similar arrangement is found in the crystal structure of the Y48H mutant (Bohren et al., 1994). The distance across the enzyme surface, from the mouth of the water channel tunnel to the mouth of the active site pocket, is approximately 20 Å, while the channel itself is approximately 9−11 Å long. The diaxial angle formed between the axes through the water channel and active site pocket is approximately 135°.

The fact that both nitrogen atoms of His110 are hydrogen bonded to water molecules, precluding assignment of the likely tautomeric state of His110, consequently inspired us to investigate theoretical methods to supplement the available experimental data. In this context, we have performed molecular modeling calculations on the binding of three substrates, D-xylose, L-xylose, and D-lyxose, in the active site of wild-type hAR and two of its site-directed mutants (H110A and H110Q). The three pentose sugars were considered suitable candidates for these experiments because of their similarity. All have the same number and types of rotatable bonds; it was therefore expected that the loss of internal entropy upon binding to the enzyme would be comparable for the three sugars and cancel. From these calculations we have been able to successfully correlate the calculated binding enthalpies with experimental Michaelis−Menten constants, and we have used this information to obtain a picture of the protonation state of His110 with these substrates bound. Additional information, such as the preferred binding conformations of D-xylose and the identification of the active site residues which contribute most significantly to the binding of D-xylose, has also been elucidated from the calculations and used to determine the most likely His110 tautomeric state.

METHODS

Preparation of the Various Enzyme/Substrate Models

Preparation of the hAR Crystal Structure for Subsequent Molecular Modeling Calculations. The high-resolution (1.65 Å) crystal structure of wild-type hAR complexed with $NADP^+$ (Wilson et al., 1992) was retrieved as entry 1ADS from the Brookhaven Protein Data Bank (Bernstein et al., 1977) and used as the starting structure for subsequent modeling experiments. Crystallographic waters which were not hydrogen bonded to the protein by at least two contacts were deleted. Protonation states at neutral pH were assigned on the basis of both atomic solvent accessibilities and salt-bridging and hydrogen-bonding opportunites. The cofactor was modeled in its reduced state with two hydrogens on atom C4 of the nicotinamide ring. Atomic partial charges and parameters for amino acids and NADPH were taken from the literature (Weiner et al., 1986; Cummins et al., 1991). Substrate atomic partial charges were obtained by first optimizing the geometry using the semiempirical Hamiltonian AM1 (Dewar et al., 1985), followed by a single point STO-3G calculation to obtain the atomic partial charges from the electrostatic potential (Singh & Kollman, 1984). The resulting enzyme model was used as the starting structure to build three different wild-type models and two mutant enzyme models.

Construction of the Five Different Enzyme Models. (i) Wild-Type Models. In order to investigate the influence of the different tautomeric states of His110 on the substrate binding affinity, three wild-type enzyme configurations were considered. In the first case His110 was configured with its Nε2 atom protonated and Nδ1 unprotonated (hereafter referred to as the HisI configuration), in the second configuration Nδ1 was protonated and Nε2 unprotonated (HisII

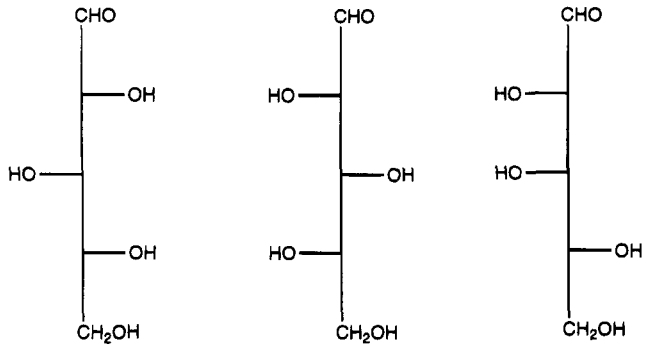

FIGURE 2: Fischer projections of the three substrates used in the modeling calculations.

configuration), and in the third both nitrogens of His110 were protonated (His+ configuration). This yielded three different wild-type enzymes (HisI, HisII, and His+).

(ii) Site-Directed Mutants. The H110A and H110Q mutants of the wild-type enzyme were constructed by replacing His110 with the appropriate residue (Ala or Gln). This procedure yielded two different mutant enzyme models (Ala and Gln).

Substrate Docking. D-Xylose, L-xylose, or D-lyxose was manually docked into the active site of each enzyme, thus ending up with 15 different ES complexes. The acyclic or open-chain structures of the three substrates are shown in Figure 2. The substrates were docked in their acyclic form, as there is strong evidence that it is this form which is used as a substrate by aldose reductase (Inagaki et al., 1982; Grimshaw, 1986). Crystallographic waters in the active site coinciding with the substrate-binding position were removed.[2] Care was taken to position the substrate's carbonyl group within hydrogen-bonding distance of the phenolic proton of Tyr48, with the aldehydic hydrogen pointing toward the six-membered ring of Trp20. In this orientation, the *re* face of the carbonyl is positioned toward and parallel with the cofactor's nicotinamide ring, so that the 4-*pro-R* hydrogen of the nicotinamide ring and the substrate's carbonyl carbon are positioned in close proximity to one another. Schematic drawings of the initial docking geometries along the carbonyl

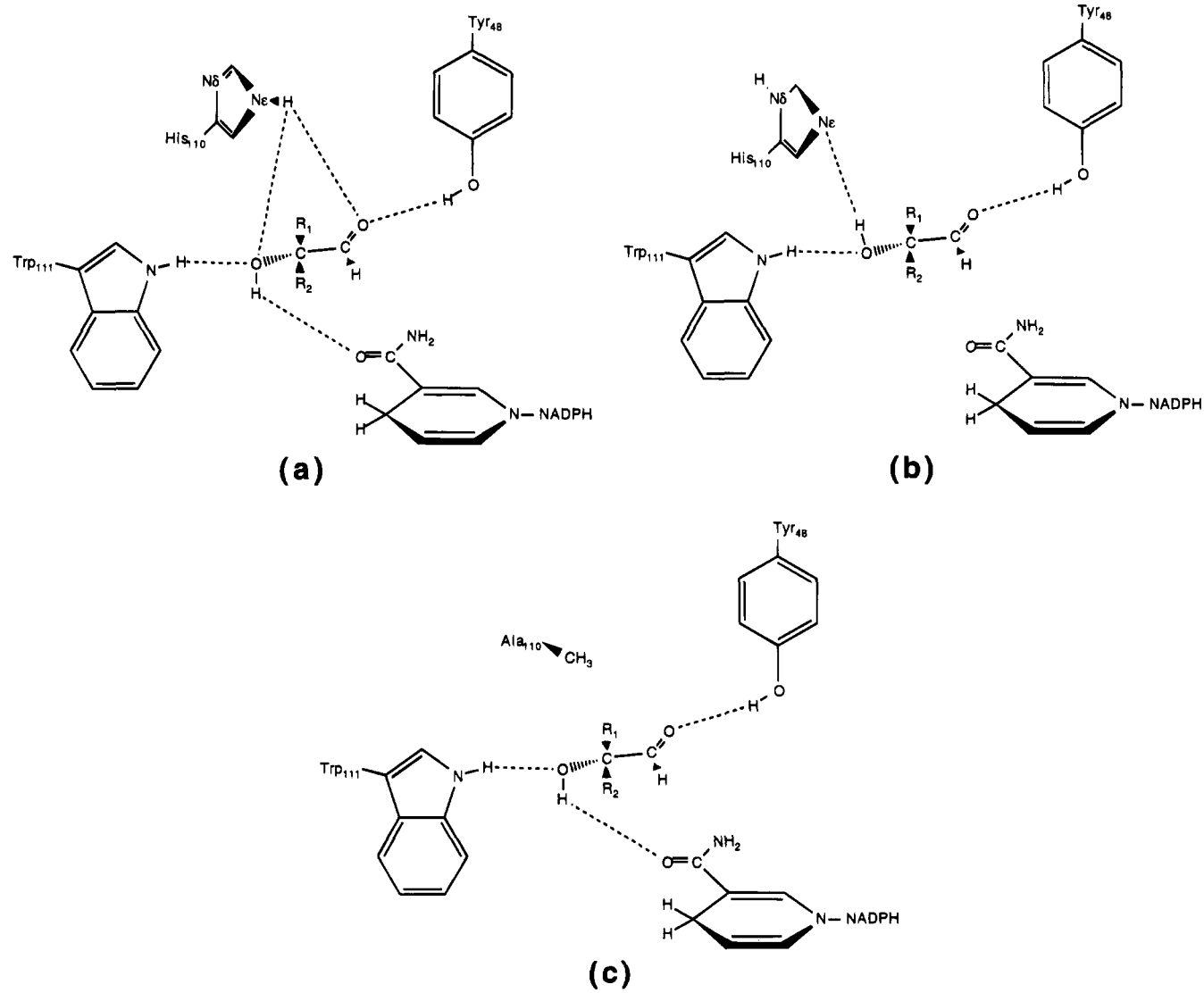

FIGURE 3: Schematic drawings of the initially docked substrates in the different enzyme active site models (hydrogen bonds represented as dotted lines). In L-xylose and D-lyxose R_1 is $-H$ and R_2 is $-[CH(OH)]_2CH_2OH$, respectively, while for D-xylose R_1 is $-[CH(OH)]_2$-CH_2OH and R_2 is $-H$. The initially docked geometry along the carbonyl and 2′-hydroxyl functionalities, shown in this figure, is identical for all three substrates but is dependent on the enzyme model. (a) Geometry initially modeled in the HisI and His+ complexes. Only the HisI enzyme is shown. In His+, His110 is doubly protonated. (b) Geometry initially adopted in HisII and Gln. Only HisII is shown. In the Gln mutant, a hydrogen bond between Gln110's Oε1 and the 2′-hydroxyl proton is initially docked. (c) Initial docking geometry for the Ala mutant. The Ala110 residue is not involved in any hydrogen bonding with the substrates.

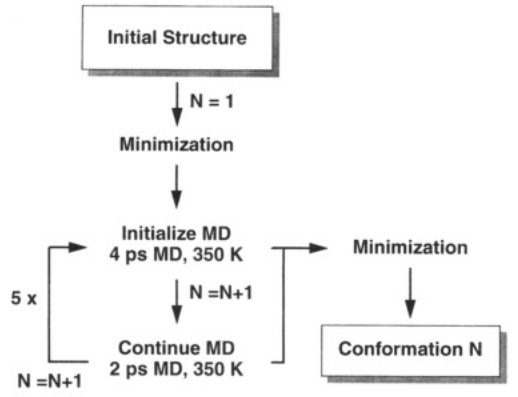

FIGURE 4: Flow chart-like representation of the MD-based conformational search procedure.

and 2′-hydroxyl group of the substrates are shown in Figure 3. The tail parts of the substrates, from atoms C3′ to C5′, were positioned so as to minimize steric overlap with the active site residues.

Addition of Counterions and Solvation of the Complexes. Charge neutralization was achieved by the addition of five sodium counterions (four for the His+ systems) and one chlorine to the complexes at positions of highest negative or positive electrostatic potential, respectively (Mark et al., 1991). Counterion positions were kept fixed during the simulations because they were positioned outside a 16 Å sphere which is centered around the phenolic proton of Tyr48 (see further). The active sites were solvated by a 18 Å spherical cap of TIP3P water molecules (Jorgensen et al., 1983), centered at the phenolic proton of Tyr48. A total of about 95 water molecules were added to each system in this fashion, and taken together with the 40 crystallographic waters this yielded a total of 135 waters.

Generation of Binding Conformations and Calculation of Interaction Enthalpies

Conformational space of the ES complexes within the active site was explored using a slightly adapted procedure of Taylor and von Itzstein (1994). A flow chart-like diagram of the procedure is shown in Figure 4. An initial energy minimization was performed to relieve steric strain associated with the newly docked ligand. Molecular dynamics (MD) was initialized by assigning random velocities taken from a Maxwell−Boltzmann distribution for a temperature of 350 K, and the simulations were then continued for 4 ps at 350 K using a temperature coupling parameter of 0.2 ps (Berendsen et al., 1984). The SHAKE algorithm (van Gunsteren & Berendsen, 1977) was used to constrain all bond lengths to their equilibrium values and to allow a rather large time step of 2 fs. The resulting structure was extracted and energy minimized. A further 2 ps of MD was performed, and the final structure was again energy minimized. This sequence was repeated five times starting at the MD initialization step, leading to ten minimized conformations for which the interaction enthalpy between E and S was calculated. This procedure was repeated for each ES complex. Essential in the procedure is the repetitive use of the MD initialization step: conformational space is sampled much more effectively this way compared to normal MD without the need to excessively heat the system (Taylor & von Itzstein, 1994). During the entire process, only the protein residues within 16 Å of the phenolic proton of Tyr48 were free to move, and the solvent molecules were restrained to their initial positions with a force constant of 0.05 kcal/(mol·Å^2) (Solmajer & Mehler, 1992). A linear distance-dependent dielectric and a residue-based nonbonded cutoff radius of 8 Å were used to avoid splitting of dipoles. Separate calculations on part of the systems but with a longer 12 Å cutoff gave almost identical interaction enthalpies and geometries (data not shown), indicating that a residue-based cutoff of 8 Å, in combination with the linear distance-dependent dielectric, is sufficient for our purposes. Energy minimization was performed until the root-mean-square derivative of the energy gradient dropped below 0.1 kcal/(mol·Å). All calculations were performed using the program AMBER 4.0 (Pearlman et al., 1991) on Silicon Graphics Indigo R4000 workstations (Silicon Graphics, Mountain View, CA) and visualized with InsightII (Biosym Technologies Inc., San Diego, CA).

Calculation of Solvation Energies

The electrostatic component of the free energies of solvation of E, S, and ES for each of the ten conformations of each ES system was obtained using the Delphi algorithm (Gilson et al., 1987; Gilson & Honig, 1988) as implemented by Biosym (Biosym Technologies Inc., San Diego, CA). In this approach, the electrostatic component of the free energy of solvation of the biomolecular system is computed by solving the Poisson−Boltzman equation using a finite difference method. The solvent-accessible surface was calculated using a probe radius of 1.8 Å and van der Waals radii of 1.1, 1.55, 1.4, 1.35, 1.88, and 1.81 Å for H, C, N, O, P, and S respectively. Atomic charges were those as described above. Solvent waters were removed, but crystallographic waters were retained. The rationale for this was that the retained crystallographic waters, which are mainly located in protein cavities or narrow channels and therefore highly restricted in their conformational freedom, are probably not well described by the dielectric constant of bulk water. To test the dependency of the results on the atomic radii, some systems were recalculated with standard Pauling radii. No significant differences in the final results for the two sets of radii were observed (data not shown). The solvation energy for ES, E, and S, respectively, was, in each case, obtained as the difference of results from two types of calculations: the first with a solvent dielectric $\epsilon = 78.6$ and the second with a solvent dielectric $\epsilon = 1$. All calculations were performed with a relative permittivity of 2 inside the protein to include solute polarizability, and the ionic strength was set to 0 mol/dm^3. The focusing method was used throughout these calculations. In this procedure, a coarse calculation is first performed using a grid 15 Å larger than the dimensions of the enzyme in each direction. The potentials thus obtained are then used in a subsequent focusing run using a smaller grid of 10 Å around the enzyme, giving a grid spacing of approximately 1 Å. This gives potential values accurate to within 5−10% (Gelpi et al., 1993). After calculation of the solvation energies, interaction enthalpies between E and S were corrected for solvation effects by adding the solvation energy of the ES complex

[2] Harrison et al. (1994) convincingly showed that the unidentified electron density in the active site of aldose reductase, previously interpreted as a water molecule in the 1.65 Å structure of Wilson et al. (1992), is instead a bound citrate molecule. The starting point for our calculations was the Wilson et al. (1992) structure. This structure obviously does not contain citrate coordinates, and therefore it was only necessary to remove the crystallographic waters in the active site of this structure prior to substrate docking.

Table 1: Average Residue Contributions to the Binding of D-Xylose to Wild-Type hAR with His 110 Modeled as HisI, HisII, and His+[a]

	av interaction enthalpy (kcal/mol)		
	HisI enzyme	HisII enzyme	His+ enzyme
His110	−6	−3	−9
Tyr48	−5	−3	−2
Trp20	−4	−4	−4
Trp111	−5	−4	−6
nicotinamide ring of NADPH	−10	−12	−9
all residues	−40	−36	−40

[a] The total binding enthalpy for each enzyme is also given.

and subtracting from it the solvation energies of E and S. The approach as outlined here has been applied by several groups to evaluate the solvation contribution to the free energy of bimolecular association [see, e.g., Honig et al. (1993) and Gilson and Honig (1988)].

RESULTS

Binding Geometry of D-*Xylose to the HisI, HisII,* and His+ *Enzymes.* Stereoviews of the ten D-xylose conformations in the active sites of HisI, HisII, and His+ are shown in Figure 5a (HisI), Figure 5b (HisII), and Figure 5c (His+). Total interaction enthalpies for the binding of D-xylose to HisI, HisII, and His+ and an analysis of the relative contributions to the binding enthalpy for a selection of the active site residues are given in Table 1.

(i) HisI. As can be seen from Figure 5a, the conformations adopted by D-xylose upon binding to hAR in the HisI configuration can be classified into two conformationally distinct clusters. The main structural difference is formed by a torsional rotation of approximately 90° around the C2′−C3′ and C3′−C4′ bonds which only affects the conformation near the C5′ end of the substrate. The absence of any suitable interactions of the hydroxyl groups at positions C4′ and C5′ of the polar substrate with the hydrophobic active site pocket of the enzyme might explain the conformational freedom in this part of the substrate. The hydroxyl groups at the C5′ end of the substrate are positioned in such a way to form favorable solvent interactions.

Major contributions to the total binding enthalpy come from the carbonyl end of D-xylose, with individual contributions of −14 kcal/mol from the carbonyl group and −17 kcal/mol from the 2′-hydroxyl group. These groups interact predominantly with the active site residues Tyr48, His110, and Trp111 and the nicotinamide ring of NADPH, with average contributions of −5, −6, −5, and −10 kcal/mol, respectively. The total of these contributions makes up almost two-thirds of the total binding enthalpy. As a result of this, tight binding along the carbonyl end of the substrate is observed, favoring only one binding conformation (Figure 5a) which is quite the opposite to the conclusion drawn about the C5′-tail end. Average distances of the hydrogen bonds between D-xylose and the active site residues are schematically shown in Figure 6.

(ii) HisII. The obvious difference between HisI (or His+) and HisII is the existence (HisI or His+) or absence (HisII) of a proton at position Nε2 of residue His110. While in HisI this proton is strongly involved in substrate binding through interactions with both the carbonyl- and 2′-hydroxyl group of the substrate, such interactions are obviously not feasible in HisII. Consequently, the average total interaction enthalpy between D-xylose and HisII is reduced by 4 kcal/mol compared to HisI. As can be seen from Figure 5b, two strong hydrogen bonds between Hε1 (of Trp111) and O2′ (of D-xylose), and O7 (of NADPH) and HO2′ (of D-xylose), are formed in all of the ten D-xylose/HisII complexes, despite the fact that a hydrogen bond between the 2′-hydroxyl group of D-xylose and Nε2 of His110 was initially modeled in our docking geometry (Figure 3b). The geometry of these two hydrogen bonds is almost identical to that of the corresponding hydrogen bonds in HisI: an average length of 1.8 Å is calculated for $O2'_{\text{D-xylose}}\cdots H\epsilon1_{\text{Trp111}}$ and $O7_{\text{NADPH}}\cdots HO2'_{\text{D-xylose}}$. In nine of the ten D-xylose/HisII complexes, a 180° rotation around the C1′−C2′ bond has occurred so that the carbonyl oxygen points to the six-membered ring of Trp20, and a hydrogen bond between the aldehydic proton and Nε2 of His110 is formed (average distance between the aldehydic hydrogen and Nε2 is 2.0 Å). In this conformation the *si* face of the carbonyl group faces the nicotinamide ring of NADPH.

(iii) His+. Although the average interaction enthalpy for the binding of D-xylose to His+ is similar to the corresponding value for HisI, detailed comparison of the binding conformations shows some remarkable differences. A plot showing the ten minimized D-xylose structures in the active site of His+ hAR is displayed in Figure 5c. The carbonyl end of D-xylose is tightly bound through interactions of the substrate's carbonyl oxygen and 2′-hydroxyl group with His110, Trp111, and the cofactor's nicotinamide ring, with distances very similar to those measured in HisI ($O1_{\text{D-xylose}}\cdots H\epsilon2_{\text{His110}}$, 2.0 Å; $O_2'_{\text{D-xylose}}\cdots H\epsilon1_{\text{Trp111}}$, 1.8 Å; $O2'_{\text{D-xylose}}\cdots H\epsilon2_{\text{His110}}$, 2.0 Å; $HO2'_{\text{D-xylose}}\cdots O7_{\text{NADPH}}$, 1.8 Å). However, the major difference between the HisI and His+ bound conformations is found for the interaction of the substrate's carbonyl oxygen with Tyr48. The distance between the carbonyl oxygen and the phenolic proton of Tyr48, which measures 2.0 Å in both HisI and the first three minimized His+ complexes, has increased to almost 5.4 Å in the last seven His+ structures. This lengthening is caused by a simultaneous displacement of both Tyr48 and Lys77 away from the positively charged His110 and a reorientation of the phenolic proton toward Asp43 instead of the substrate's carbonyl oxygen. Inspection of the evolution of the nonbonded interaction enthalpies between His110 and both Tyr48 and Lys77 reveals that the observed residue displacement is partially driven by unfavorable interactions with the positively charged His110 (data not shown). An obvious consequence of the observed rearrangement of the phenolic proton of Tyr48 is a decreased binding interaction with D-xylose. While the average interaction enthalpy for the first three minimized structures is −48 kcal/mol, an increase to a less favorable average interaction enthalpy of −37 kcal/mol in the remaining seven complexes is calculated. It is therefore likely that this latter figure represents the actual interaction enthalpy more accurately than does the average of all of the ten enthalpies.

Correlation between Interaction Enthalpies and Experimental log(K_m) or log(k_{cat}/K_m) Values. Michaelis−Menten constants K_m and specificity constants k_{cat}/K_m derived from kinetic studies for the binding of D-xylose, L-xylose, and D-lyxose to the three hAR enzymes (Bohren et al., 1994) and the corresponding calculated interaction enthalpies with and without solvation free energy corrections are presented in Table 2. A plot of the experimental log(K_m) values against the interaction enthalpies for the binding of each of the three

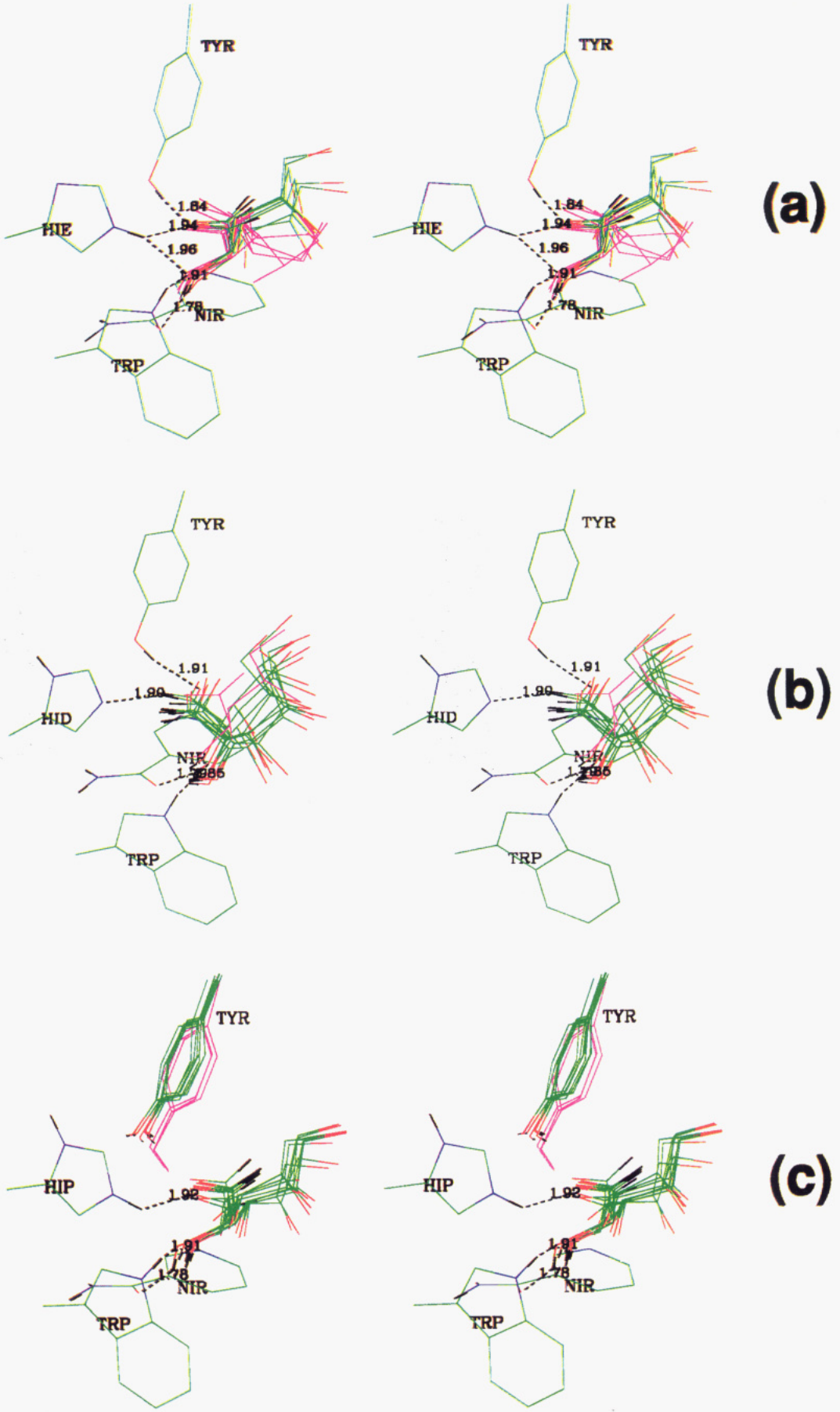
TYR
HIE
1.84
1.94
1.96
1.91
1.78
NIR
TRP
(a)
TYR
HIE
1.84
1.94
1.96
1.91
1.78
NIR
TRP
TYR
HID
1.91
1.99
NIR
TRP
(b)
TYR
HID
1.91
1.99
NIR
TRP
TYR
HIP
1.92
1.91
1.78
NIR
TRP
(c)
TYR
HIP
1.92
1.91
1.78
NIR
TRP

FIGURE 5: (a) Stereo plot of the ten minimized binding conformations of D-xylose in the active site of hAR with His110 in the HisI tautomeric form (only Nε2 protonated). The averaged geometries of the active site residues Trp111 (TRP), His110 (HIE), and Tyr48 (TYR) and the nicotinamide ring of NADPH (NIR) are also shown. For clarity, only the polar hydrogens on the enzyme residues and the aldehydic and the 2′-hydroxyl proton of D-xylose are shown. Two different color patterns are used to highlight the two distinct conformational clusters along the tail part of the substrate: atom color coding (H, black; O, red; C, green; N, blue) is used for the major cluster; magenta coloring is used to display the minor family which differs from the main family by a 90° rotation around the C2′−C3′ and C3′−C4′ bonds. Although conformational freedom is observed along the tail part of the D-xylose, the carbonyl and 2′-hydroxyl functionalities are tightly bound in the active site, and identical conformations along this site are found for all of the ten members. Hydrogen bonds are indicated by dotted lines; as an indication, the interatomic distances calculated for the first complex are shown. (b) As for (a) but with His110 in the HisII tautomeric form (only Nδ1 protonated, HID). In contrast to the binding of D-xylose to the HisI enzyme, a 180° rotation around the C1′−C2′ bond has occurred in nine out of the ten D-xylose substrates (atom-colored molecules). This orients the aldehydic proton toward the Nε2 of His110. The only molecule for which this reorientation has not taken place is colored in magenta. Also note the involvement of the substrate's 2′-hydroxyl group in hydrogen bonds with both O7 of NADPH and Hε1 of Trp111. (c) As for (a) but with His110 in the His+ tautomeric form (doubly protonated, HIP). All of the ten Tyr48 conformations are drawn to show the reorientation of this residue during the course of the simulation. The first three sampled Tyr48 conformations are colored in magenta; the remaining seven are colored by atom. The phenolic proton, initially docked to form a hydrogen bond with the carbonyl oxygen of the substrate, is reoriented away from the substrate during the course of the simulation.

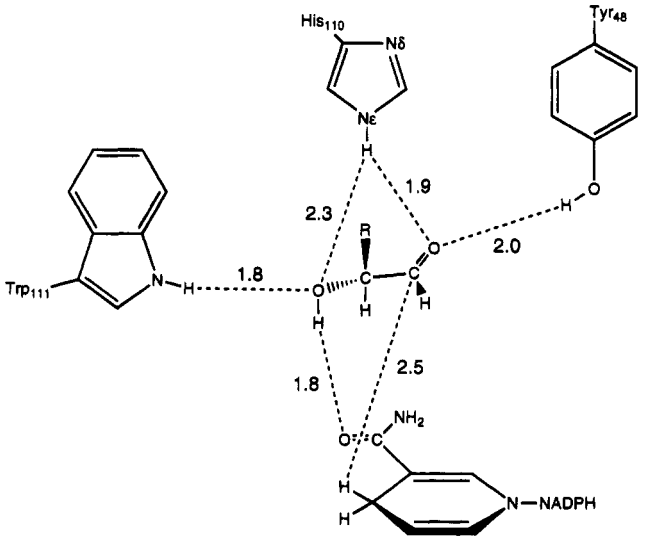

FIGURE 6: Schematic drawing of the predicted binding geometry of D-xylose to the active site of wild-type human aldose reductase. Shown are the three active site residues which make up the majority of the total binding enthalpy and the nicotinamide ring of NADPH. Distances, which are averaged values over the ten minimized structures, are in angstroms.

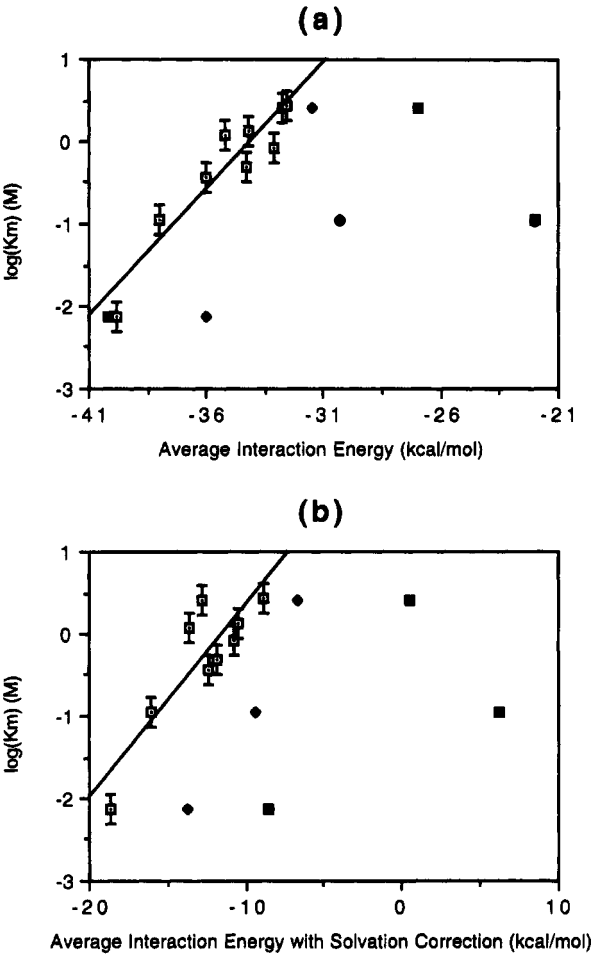

FIGURE 7: (a) Plot of the average interaction enthalpies against the experimental log(K_m) values for the 18 enzyme/substrate complexes. The nine points which were used for the calculation of the linear regression line are shown by open squares with black dots. The equation of the fitted line is log(K_m) = 10.5 + 0.31IE, in which IE stands for interaction enthalpy. Solid diamonds show the corresponding values of the binding between the HisII configuration enzymes with either D-xylose, L-xylose, or D-lyxose. Black squares are used to mark the values of the His+ complexes with the three substrates. Error bars for the experimental log(K_m) values are also shown. (b) As for (a) except that solvation corrections were applied to the interaction enthalpies. The equation of the fitted line is now log(K_m) = 2.72 + 0.24IE, in which IE stands for interaction enthalpy.

substrates to each of the three enzymes (wild-type enzyme/Gln mutant/Ala mutant) is shown in Figure 7. Correlation coefficients for the experimental log(K_m) values against the calculated interaction enthalpies for the binding of each of the three substrates (D-xylose, L-xylose, and D-lyxose) to each of the three hAR enzymes (wild-type and H110Q and H110A mutants) are shown in Table 3. A good correlation is found, irrespective of whether solvation corrections are taken into account, only when the wild-type enzyme is modeled in the HisI form [correlation coefficient r = 0.94 (no solvation corrections) and 0.87 (with solvation corrections)]. No significant correlation is apparent for the two other tautomers of His110 (HisII, r = 0.32 and 0.55; His+, r = 0.28). A similar conclusion can be reached from the correlation constants obtained for the log(k_{cat}/K_m) values (Table 4).

In order to assess the significance of the above derived correlation between interaction enthalpies and measured parameters, its success in predicting the K_m of D-glucose was investigated. D-Glucose was considered to be a suitable candidate because of its structural resemblance with D-xylose, L-xylose, and D-lyxose. An average interaction enthalpy for D-glucose, which includes solvation corrections, of −15 kcal/mol was calculated for the binding of D-glucose to the HisI enzyme using the method as described earlier. Using the regression equation for HisI (given in the caption of Figure 7b), a log(K_m) for D-glucose of −0.93 M was calculated, which is, within error limits, equal to the experimental value of −0.94 M (Bohren et al., 1991). In contrast, the values

Table 2: Comparison between Experimental $\log(K_m)$ and $\log(k_{cat}/K_m)$ Values and Calculated Interaction Enthalpies (with and without Solvation Corrections) for the Different Enzyme/Substrate (ES) Complexes[a]

ES system[b]	kinetic parameters[c] $\log(K_m)$	kinetic parameters[c] $\log(K_{cat}/K_m)$	av (max/min) ΔH_{inter}[d]	av (max/min) $\Delta H_{inter} + \Delta\Delta G_{sol}$[e]
D-xylose/His[f]	−2.131	1.732	−40 (−44.8/−34.6) (I), −36 (−37.8/−33.5) (II), −40 (−52.8/−35.2) (+)	−19 (−21.4/−14.7) (I), −14 (−15.6/−12.2) (II), −9 (−19.8/+3.0) (+)
D-xylose/Gln	−0.065	−1.201	−33 (−36.3/−27.2)	−11 (−14.4/−5.6)
D-xylose/Ala	0.127	−1.886	−34 (−38.4/−29.1)	−10 (−13.5/−6.7)
L-xylose/His[f]	−0.955	0.322	−38 (−40.2/−35.7) (I), −30 (−34.1/−25.0) (II), −22 (−27.8/−17.0) (+)	−16 (−17.3/−14.8) (I), −9 (−11.5/−4.0) (II), +6 (+1.0/+10.7) (+)
L-xylose/Gln	0.076	−2.229	−35 (−38.4/−31.9)	−14 (−17.2/−8.8)
L-xylose/Ala	−0.444	0.003	−36 (−39.8/−30.0)	−12 (−16.0/−8.0)
D-lyxose/His[f]	0.420	−1.222	−33 (−37.0/−29.5) (I), −32 (−33.2/−29.2) (II), −27 (−31.8/−22.4) (+)	−13 (−16.7/−8.5) (I), −7 (−10.2/−4.0) (II), +1 (−6.0/+4.8) (+)
D-lyxose/Gln	−0.296	−1.854	−34 (−36.3/−32.8)	−12 (−13.8/−8.7)
D-lyxose/Ala	0.438	−2.699	−33 (−35.1/−31.0)	−9 (−12.4/−6.0)

[a] Shown are the average, maximum, and minimum interaction enthalpies (with or without corrections for differences in solvation free energies) for the interaction between each of the enzymes with each of the substrates. [b] D-Xylose/His, L-xylose/His, and D-lyxose/His, complexes between wild-type hAR and D-xylose, L-xylose, and D-lyxose, respectively; D-xylose/Gln, L-xylose/Gln, and D-lyxose/Gln, complexes between the H110Q mutant of hAR and D-xylose, L-xylose, and D-lyxose, respectively; D-xylose/Ala, L-xylose/Ala, and D-lyxose/Ala, complexes between the H110A mutant of hAR and D-xylose, L-xylose, and D-lyxose, respectively. [c] From Bohren et al. (1994). Values for $\log(K_m)$ are in M and for $\log(k_{cat}/K_m)$ in M^{-1} s^{-1}. [d] Average interaction enthalpy between E and S obtained from averaging over the ten ES conformations. Values in parentheses are the maximum/minimum interaction enthalpies of the set of 10, *i.e.*, the most/least favorable enthalpies found in the set of 10 values. Values are in kcal/mol. [e] As for footnote *d* but corrected for differences in solvation free energies. Values are in kcal/mol. [f] Three tautomeric states of His110 were examined: His110 with only Nε2 protonated (I), His110 with only Nδ1 protonated (II), or His110 doubly protonated (+).

Table 3: Correlation Coefficients from a Linear Least-Squares Fit between the Experimental $\log(K_m)$ Values and the Calculated Interaction Enthalpies (with and without Solvation Corrections) for the Binding of the Three Substrates (D-Xylose, L-Xylose, and D-Lyxose) to the Three hAR Enzymes (Wild Type and H110Q and H110A Mutants)[a]

ES system	$\log(K_m)$ *versus* ΔH_{inter}[b] av[g]	$\log(K_m)$ *versus* ΔH_{inter}[b] max (min)[h]	$\log(K_m)$ *versus* $(\Delta H_{inter} + \Delta\Delta G_{sol})$[c] av[i]	$\log(K_m)$ *versus* $(\Delta H_{inter} + \Delta\Delta G_{sol})$[c] max (min)[j]
HisI[d]	0.94	0.90 (0.68)	0.87	0.79 (0.84)
HisII[e]	0.32	0.23 (0.19)	0.55	0.31 (0.61)
His+[f]	0.28	0.62 (0.17)		

[a] The results for the three protonation states of His110 (HisI, HisII, His+) are compared. [b] The interaction enthalpies ΔH_{inter} were used to calculate the correlation coefficients. [c] The interaction enthalpy corrected for differences in solvation energies $(\Delta H_{inter} + \Delta\Delta G_{sol})$ was used to calculate the correlation coefficients. [d] Correlation coefficients between the experimental $\log(K_m)$ values and interaction enthalpies (with or without solvation corrections) as calculated for the binding of each of the three substrates (D-xylose, L-xylose, D-lyxose) with each of the following enzymes: wild-type hAR with His110 in the HisI configuration (only Nε2 protonated), H110Q mutant, and H110A mutant. [e] As for footnote *d* except that the wild-type enzyme is modeled with His110 in the HisII configuration (only Nδ1 protonated). [f] As for footnote *d* except that the wild-type enzyme is modeled with His110 in the His+ configuration (Nδ1 and Nε2 both protonated). [g] The average value of the ten interaction enthalpies calculated for each ES complex was used to calculate the correlation coefficient. [h] The maximum and minimum (within parentheses) values (*i.e.*, the most favorable and least favorable, respectively) of the ten interaction enthalpies calculated for each ES complex were used to calculate the correlation coefficient. [i] The average value of the ten $(\Delta H_{inter} + \Delta\Delta G_{sol})$ calculated for each ES complex was used to calculate the correlation coefficient. The correlation coefficient for the His+ enzyme was not calculated. [j] The maximum and minimum (within parentheses) values (*i.e.*, the most favorable and least favorable, respectively) of the ten solvation-corrected enthalpies $(\Delta H_{inter} + \Delta\Delta G_{sol})$ calculated for each ES complex were used to calculate the correlation coefficient. The correlation coefficient for the His+ enzyme was not calculated.

Table 4: Correlation Coefficients from a Linear Least-Squares Fit between the Experimental $\log(k_{cat}/K_m)$ Values and the Calculated Interaction Enthalpies (with and without Solvation Corrections) for the Binding of the Three Substrates (D-Xylose, L-Xylose, and D-Lyxose) to the Three hAR Enzymes (Wild Type and H110Q and H110A Mutants)[a]

ES system	$\log(k_{cat}/K_m)$ *versus* ΔH_{inter}[b] av[g]	$\log(k_{cat}/K_m)$ *versus* ΔH_{inter}[b] max (min)[h]	$\log(k_{cat}/K_m)$ *versus* $(\Delta H_{inter} + \Delta\Delta G_{sol})$[c] av[i]	$\log(k_{cat}/K_m)$ *versus* $(\Delta H_{inter} + \Delta\Delta G_{sol})$[c] max (min)[j]
HisI[d]	−0.86	−0.89 (−0.49)	−0.85	−0.82 (−0.79)
HisII[e]	−0.17	−0.12 (0.06)	−0.30	−0.13 (0.60)
His+[f]	−0.09	−0.46 (0.10)		

[a] The results for the three protonation states of His110 (HisI, HisII, His+) are compared. [b] The interaction enthalpies ΔH_{inter} were used to calculate the correlation coefficients. [c] The interaction enthalpy corrected for differences in solvation energies $(\Delta H_{inter} + \Delta\Delta G_{sol})$ was used to calculate the correlation coefficients. [d] Correlation coefficients between the experimental $\log(k_{cat}/K_m)$ values and interaction enthalpies (with or without solvation corrections) as calculated for the binding of each of the three substrates (D-xylose, L-xylose, D-lyxose) with each of the following enzymes: wild-type hAR with His110 in the HisI configuration (only Nε2 protonated), H110Q mutant, and H110A mutant. [e] As for footnote *d* except that the wild-type enzyme is modeled with His110 in the HisII configuration (only Nδ1 protonated). [f] As for footnote *d* except that the wild-type enzyme is modeled with His110 in the His+ configuration (Nδ1 and Nε2 both protonated). [g] The average value of the ten interaction enthalpies calculated for each ES complex was used to calculate the correlation coefficient. [h] The maximum and minimum (within parentheses) values (*i.e.*, the most favorable and least favorable, respectively) of the ten interaction enthalpies calculated for each ES complex were used to calculate the correlation coefficient. [i] The average value of the ten $(\Delta H_{inter} + \Delta\Delta G_{sol})$ calculated for each ES complex was used to calculate the correlation coefficient. The correlation coefficient for the His+ enzyme was not calculated. [j] The maximum and minimum (within parentheses) values (*i.e.*, the most favorable and least favorable, respectively) of the ten solvation-corrected enthalpies $(\Delta H_{inter} + \Delta\Delta G_{sol})$ calculated for each ES complex were used to calculate the correlation coefficient. The correlation coefficient for the His+ enzyme was not calculated.

determined from the interaction enthalpies for the other His110 tautomers deviate significantly from experiment: 0.71 and −0.31 M was calculated for HisII and His+, respectively. It should be pointed out that this comparison does not take into consideration that the percentage of the free aldehyde form of D-glucose is roughly 10-fold less than that of the three pentoses (D-xylose, L-xylose, and D-lyxose). However, correction for variance in free aldehyde content will not significantly alter the conclusions because the difference between calculated and corrected $\log(K_m)$ for D-glucose will always remain smaller for HisI than for the other two His110 configurations.

DISCUSSION

Inspection of the calculated binding geometries of D-xylose to hAR reveals some remarkable differences between the HisI, HisII, and His+ forms of the enzyme and suggests that His110 is mainly found in a HisI-like tautomeric state when aldehyde substrate is bound. In particular, three distinct points can be discussed from our data. First, the binding geometry of D-xylose observed in the HisI from of hAR is closer to what we might expect from mechanistic considerations than is the geometry calculated for the HisII and His+ enzymes. Significantly, the reactive carbon of the aldehyde group of D-xylose is closely positioned to the 4-*pro-R* hydrogen of NADPH (average distance 2.5 Å), and it might be expected that such a close distance facilitates hydride transfer from NADPH to the carbonyl carbon. Furthermore, short hydrogen bond distances of only 1.9 and 2.0 Å between the aldehydic oxygen of the substrate and the protons of His110 and Tyr48, respectively, could facilitate proton transfer or might enhance the polarization of the carbonyl function. The corresponding distances in the HisII and His+ geometries are much less favorable in this regard. Second, the geometries calculated in the HisI form of the enzyme orient the *re* face of the aldehydic group toward the nicotinamide ring of the cofactor. This observation is in agreement with experimental data because it leads to products of the correct proenantiomeric form (vander Jagt et al., 1992). In contrast to this, a 180° twist around the C1′−C2′ bond occurs in the majority of the conformations calculated for the binding of D-xylose to the HisII form of hAR. Such a rotation positions the *si* face of the carbonyl group toward the nicotinamide ring of NADPH, which is not consistent with experiment as this would lead to the incorrect proenantiomeric products (vander Jagt et al., 1992). Third, in the His+ enzyme model, a displacement of Tyr48 away from the positively charged His110 is observed, which results in an important decrease in the contribution of this residue to the total binding enthalpy of D-xylose. This would imply that Tyr48 should be of little relevance in the binding of substrates when His110 was configured as His+. However, the dramatic drop in both K_m and k_{cat} for the site-directed Y48F mutant compared to the corresponding wild-type parameters (Tarle et al., 1993; Bohren et al., 1994) suggests not only that Tyr48 is crucial in the mechanism of catalysis but also that the residue is involved in substrate binding. Therefore, the calculated geometry for the binding of D-xylose to hAR with His110 in the His+ configuration is not in agreement with what we would expect from experimental observations. The conclusion that His110 is probably not doubly protonated has also been reached by others (Wilson et al., 1992; Bohren et al., 1994). This conclusion is based on the fact that His110 is positioned in a predominantly hydrophobic area and in close proximity to a positively charged Lys77. Such an environment is not considered conducive to the formation of a positively charged imidazolium group under normal pH conditions.

Our calculations on the HisI form of the enzyme suggest that Trp111 participates in the binding of 2′-hydroxyl-containing aldehyde substrates. In particular, an average contribution of −5 kcal/mol was calculated for this residue, and the majority of this is achieved through hydrogen-bonding interactions with the substrate's 2′-hydroxyl group. Although we have no experimental data to verify the role of Trp111 in substrate binding, it is nevertheless interesting to note that Trp111 is also conserved in aldehyde reductase (ALR1), where it occupies almost exactly the same position in the active site (El-Kabbani, private communication).

It has been shown that a linear relationship between free energies of substrate binding and $\log(K_m)$ or $\log(k_{cat}/K_m)$ values can exist [see, e.g., Fersht (1985)]. In the present work on hAR, we have demonstrated a similar relationship between substrate/enzyme interaction enthalpies and measured parameters [$\log(K_m)$ or $\log(k_{cat}/K_m)$] when the active site residue His110 was modeled with the Nϵ2 atom protonated and Nδ1 unprotonated. No correlation was found for the other two His110 configurations. Although we are unable to postulate on the extent of such a relationship, it is not unreasonable to suggest that the conformations of the ES complexes calculated for the HisI enzyme are indeed a reflection of the S conformation adopted just before the actual reduction step takes place.[3] Therefore, our calculations strongly suggest that, in wild-type hAR, the Nϵ2 atom of His110 is protonated when aldehyde substrate is bound, while the two other tautomeric states appear to be much less likely. In addition, the substrate's 2′-hydroxyl group always forms a hydrogen bond with O7 of NADPH and Hϵ1 of Trp111. Thus, according to our model, the stereocontrol of hAR is significantly orchestrated by both Trp111 and the amide side chain of the NADPH nicotinamide ring.

We have shown that the Nϵ2 atom of His110 is protonated when aldehyde substrates bind to the hAR/NADPH complex. The availability of a proton at Nϵ2 suggests that His110 is also a possible candidate to serve as the proton donor group in the reduction reaction catalyzed by hAR. However, because we, among others (Wilson et al., 1992; Bohren et al., 1994), have shown that a doubly protonated His110 residue is rather unlikely, the donation of a proton by His110 to the substrate's carbonyl oxygen would imply the unlikely formation of a negatively charged imidazolium ion. Nevertheless, our results do not exclude the possibility of His110 acting as the proton donor residue, provided that a charge-release mechanism is available which can provide a proton to the Nδ1 atom of His110 when Nϵ2 is deprotonated during the course of the reaction. It is interesting to speculate that the chain of conserved hydrogen-bonded water molecules in hAR (see above), linking the Nδ1 nitrogen of His110 to the solvent-accessible surface of the enzyme, might supply such a charge-release mechanism by transferring protons from bulk solvent to the Nδ1 of His110. However, detailed kinetic experiments are required to test this hypothesis. Further work is currently in progress to investigate the effects of designed ligands which bind in this channel.

ACKNOWLEDGMENT

We are grateful to Dr. Jill E. Gready (University of Sydney) for providing us with the charges and parameters of the NADPH cofactor. Jeff Dyason is gratefully acknowl-

[3] One of the referees has quite correctly pointed out that the observed correlation between the calculated interaction enthalpy and either K_m or k_{cat}/K_m should be a direct reflection of the ground-state enthalpy for the aldehyde binding to the enzyme/NADPH complex. Specifically, k_{cat} should be constant for all three pentoses, because the release of $NADP^+$ is rate-limiting in the aldehyde reduction reaction for native aldose reductase and therefore implies that k_{cat} = $NADP^+$ release rate. Also, the apparent K_m for aldehyde becomes equal to the rate constant for $NADP^+$ release divided by the on-rate for aldehyde binding: K_m = ($NADP^+$ release rate)/(aldehyde on-rate). Thus, it follows directly that k_{cat}/K_m = aldehyde on-rate.

edged for his help with computer support. We thank Dr. Ossama El-Kabbani (University of Alabama at Birmingham) for providing us with preliminary information on the crystal structure of ALR1. Dr. Charles E. Grimshaw (The Whittier Institute for Diabetes and Endocrinology, La Jolla) is acknowledged for many interesting and helpful discussions. Finally, one of the referees is acknowledged for pointing out the work of Flynn et al. (1975) regarding the stereochemistry for hydride addition in ALR1 and for pointing out that the observed correlation between calculated interaction enthalpy and either K_m or k_{cat}/K_m should be a direct reflection of the ground-state enthalpy for aldehyde binding to the enzyme/NADPH complex.

REFERENCES

Berendsen, H. J. C., Postma, J. P. M., van Gunsteren, W. F., DiNola, A., & Haak, J. R. (1984) *J. Chem. Phys. 81*, 3684−3690.

Bernstein, F. C., Koetzle, T. F., Williams, G. B., Meyer, G. F., Price, M. D., Rodgers, J. R., Kennard, O., Shimanouchi, T., & Tasumi, M. (1977) *J. Mol. Biol. 122*, 535−542.

Bohren, K. M., Bullock, B., Wermuth, B., & Gabbay, K. H. (1989) *J. Biol. Chem. 264*, 9547−9551.

Bohren, K. M., Page, J. L., Shankar, R., Henry, S. P., & Gabbay, K. H. (1991) *J. Biol. Chem. 266*, 24031−24037.

Bohren, K. M., Grimshaw, C. E., Lai, C.-J., Harrison, D. H., Ringe, D., Petsko, G. A., & Gabbay, K. H. (1994) *Biochemistry 33*, 2021−2032.

Cummins, P. L., Ramnarayan, K., Singh, U. C., & Gready, J. E. (1991) *J. Am. Chem. Soc. 113*, 8247−8256.

Davenport, R. C., Bash, P. A., Seaton, B. A., Karplus, M., Petsko, G. A., & Ringe, D. (1991) *Biochemistry 30*, 5821−5826.

Dewar, M. J. S., Zoebisch, E. G., Healy, E. F., & Stewart, J. J. P. (1985) *J. Am. Chem. Soc. 107*, 3902−3909.

Fersht, A. (1985) *Enzyme structure and mechanism*, W. H. Freeman & Co., New York.

Flynn, T. G., & Green, N. C. (1993) in *Enzymology and Molecular Biology of Carbonyl Metabolism* (Weiner, H., Crabb, D. W., & Flynn, T. G., Eds.) Vol. 4, pp 251−257, Plenum Press, New York.

Flynn, T. G., Shires, J., & Walton, D. J. (1975) *J. Biol. Chem. 250*, 2933−2940.

Gelpi, J. L., Jackson, R. M., & Holbrook, J. J. (1993) *J. Chem. Soc., Faraday Trans. 89*, 2707−2716.

Gilson, M. K., & Honig, B. H. (1988) *Proteins 4*, 7−18.

Gilson, M. K., Sharp, K. A., & Honig, B. H. (1987) *J. Comput. Chem. 9*, 327−335.

Grimshaw, C. E. (1986) *Carbohydr. Res. 148*, 345−348.

Harrison, D. H., Bohren, K. M., Ringe, D., Petsko, G. A., & Gabbay, K. H. (1994) *Biochemistry 33*, 2011−2020.

Honig, B., Sharp, K., & Yang, A.-S. (1993) *J. Phys. Chem. 97*, 1101−1109.

Inagaki, K., Miwa, I., & Okuda, J. (1982) *Arch. Biochem. Biophys. 216*, 337−344.

Jorgensen, W. L., Chandrasekhar, J., Madura, J. D., Impey, R. W., & Klein, M. L. (1983) *J. Chem. Phys. 79*, 926−935.

Kador, P. F. (1988) *Med. Res. Rev. 8*, 325−352.

Mark, A. E., Berendsen, H. J. C., & van Gunsteren, W. F. (1991) *Biochemistry 30*, 10866−10872.

Masson, E. A., & Boulton, A. J. M. (1990) *Drugs 39*, 190−202.

Pearlman, D. A., Case, D. A., Caldwell, J. C., Seibel, G. L., Singh, U. C., Weiner, P., & Kollman, P. A. (1991) *AMBER 4.0*, University of California, San Francisco.

Singh, U. C., & Kollman, P. A. (1984) *J. Comput. Chem. 5*, 129−145.

Sitkoff, D., Sharp, K. A., & Honig, B. (1994) *J. Phys. Chem. 98*, 1978−1988.

Solmajer, T., & Mehler, E. L. (1992) *Int. J. Quantum Chem. 44*, 291−299.

Tarle, I., Borhani, D. W., Wilson, D. K., Quiocho, F. A., & Petrash, J. M. (1993) *J. Biol. Chem. 268*, 25687−25693.

Taylor, N. R., & von Itzstein, M. (1994) *J. Med. Chem. 37*, 616−624.

vander Jagt, D. L., Robinson, B., Taylor, K. K., & Hunsaker, L. A. (1992) *J. Biol. Chem. 267*, 4364−4369.

van Gunsteren, W. F., & Berendsen, H. J. C. (1977) *Mol. Phys. 34*, 1311−1327.

Weiner, S. J., Kollman, P. A., Nguyen, D. T., & Case, D. A. (1986) *J. Comput. Chem. 7*, 230−252.

Wermuth, B., Bürgisser, H., Bohren, K., & Von Wartburg, J.-P. (1982) *Eur. J. Biochem. 127*, 279−284.

Wilson, D. K., Bohren, K. M., Gabbay, K. H., & Quiocho, F. A. (1992) *Science 257*, 81−84.

BI942922I